PCCP

Accepted Manuscript

ROYAL SOCIETY OF CHEMISTRY

www.rsc.org/pccp

Tuning Spin Polarization and Spin Transport of Zigzag Graphene Nanoribbons by Line Defects

G. P. Tang*, Z. H. Zhang*, X. Q. Deng, Z. Q. Fan, and H. L. Zhu

Institute of nanomaterial & nanostructure, Changsha University of science and technology, Changsha 410114, China

Abstract

From first-principles methods, the spin-dependent electronic properties of zigzag-edged graphene nanoribbons (ZGNRs) with a line defect (558-defect) are investigated systematically and compared to those of the pristine ZGNR. Results show that the line defect possesses an obvious tuning effect on the spin-polarization of the edge carbon atoms of the defective ZGNRs, and the spin-polarization and spin-transport are sensitive to the position of line defect. The defective ZGNRs can realize a transition from antiferromagnetism (AFM) to ferrimagnetism and ferromagnetism (FM) via changing the position of line defect from center to the zigzag edge of ZGNRs. More importantly, when the line defect is located at the one edge, the defective ZGNRs exhibit the long-range magnetic ordering at edges with a high Curie temperature up to 276K, and the defective ZGNR system can generate high-performance spin-filter effect in the large bias range, 0.0～0.5V. Such a sensitive modulation for the spin-polarization and spin-transport holds great promise for applications of the graphene-based systems in nano-scale spintronic devices.

* Address correspondence to guipingtang@163.com (G. P. Tang) and cscuzzh@163.com (Z H. Zhang).

1. Introduction

Nanostructured magnetic materials have a wide range of applications in the field of spintronics. There have been continuing efforts in searching for new magnetic nanomaterials, and much recent interest has been devoted to magnetism of carbon-based, especially graphene-based structures [1–6]. Graphene has a fairly simple honeycomb atomic structure, rather unique electronic structure, long spin relaxation lenth and liftime, and can be used as a excellent ballistic spin transport channel [7–10]. The magnetic graphene nanostructures are particularly promising for spintronics applications, a very probable future step in the evolution of electronics industry, which promises information storage, processing and communication at a faster speed and with a lower energy consumption [11–13]. Although the pristine two-dimensional (2D) infinite graphene sheet is nonmagnetic (NM), zigzag-edged graphene nanoribbons (ZGNRs) have magnetic edges as a result of electrons spin polarization, which have been theoretically predicted and experimentally confirmed [14–17]. Magnetic zigzag edges of graphene are considered as a basis for novel spintronics devices. However, for the ground-state electronic configurations of ZGNRs, the spin polarization at the two edges have an opposite orientation [18], the antiferromagnetic coupling results in no net magnetic moment in the system. This hinders further applications of ZGNRs in spintronics. In addition, the spin-resolved edge magnetism of ZGNRs has been found to be highly unstable owing to lacking the long-range magnetic ordering with a good transition temperature, thus also making it difficult for spintronics applications under ambient conditions, which is also the primary factor that the feasibility of the proposed nanoscale spintronics devices currently based on graphene edge magnetism is questioned [19, 20]. Therefore it is highly desirable to tune the spin polarization at edges of ZGNRs for realizing transition from antiferromagnetism (AFM) to ferromagnetism (FM), and establishing the long-range magnetic ordering at edges with a high Curie temperature.

Currently, a few possible methods have been proposed [21–27], but how to achieve on experiment remain challenges. For example, Sawada *et al.* found that injecting carriers (electrons or holes) to ZGNR can yield a ferromagnetic coupling between the two edges [21]. Transition to FM can also be induced by the substrate magnetic field when ZGNRs are deposited on graphene/Ni(111) surface [22]. However, the exchange energies are very small.

Xu *et al*. demonstrated that the transition to FM is possible when one carbon atom at one edge is saturated by two H atoms and that at the other edge by one H [26], but such a precise control is not easy experimentally.

One of the alternative approaches is to introduce extended defects into the graphene lattice [28–33]. The topological line defects composed of octagons and fused pentagons have been observed experimentally in graphene sheets (see **figure 1**(b)) [28]. The presence of the line defect makes the graphene sheet show the metallic character, which is consistent with the theory proposed by Yazyev et al. based on the momentum conservation rule [34]. When the line defect is introduced into ZGNRs, the presence of localized states in the line defect may have different effects on the electronic states of the two spins and change the magnetic behavior of the system. In the present work, using the first-principles approach, we investigate systematically the impact of a line defect on spin-dependent electronic properties of ZGNRs. We try to tune the spin-polarization and spin-transport of ZGNRs via an introduced line defect, and explore the Curie temperature and spin-filter effect for the ZGNRs with the line defect.

2. Models and methods

The ZGNR model we study is shown in figure 1, which contains the 558-defect line, where there are *N* zigzag carbon chains across the width, denoted as 558-defect-*N*-ZGNR. After relaxation, the system retains its planar structure, the C-C bond lengths of pentagonal and octagonal rings are within 1.41～1.45Å , indicating delocalized π bonding. To simplify the investigation, we only consider three different-width ZGNRs with *N*=7, 9, and 11, respectively, and mainly focus on the case of *N*=9. Choosing four different unit supercells for each case, namely, ZGNR corresponds the perfect graphene nanoribbon, and M1, M2, and M3 correspond a line defect at center, next-closest to the edge, closest to the edge, respectively.

We consider well-fledged first-principles calculations using the density functional theory (DFT), we expect it to provide the most detailed and accurate description of the electronic properties. The geometry optimization and electronic properties are calculated by using the non-equilibrium Green's function (NEGF) method combined with the density functional theory (DFT) as implemented in Atomistix ToolKit (ATK). The generalized gradient approximation (GGA) and the double-zeta polarized basis set (DZP) are used. The

convergence criteria of energy and force are set to 1×10^{-5}eV and 0.01eV/Å, respectively. The k-point sampling is 1×10×100, the cutoff energy is set to 150 Ry, and the electron temperature is fixed at 300K. The spin-resolved current I_σ under bias voltage V_b is calculated with the Landauer-Büttiker formula:

$$I_\sigma(V_b)=\frac{e}{h}\int T_\sigma\left(E,V_b\right)\left[f_L\left(E,V_b\right)-f_R\left(E,V_b\right)\right]dE \qquad (1)$$

where $T_\sigma(E,V_b)$ is the spin-resolved transmission probability, $f_{L/R}(E,V_b)$ is the Fermi–Dirac distribution function of the left (L)/right (R) electrode, and σ is a spin index(↑, ↓). The non collinear spin orientation effect is neglected due to the absence of magnetic domain wall in our calculations.

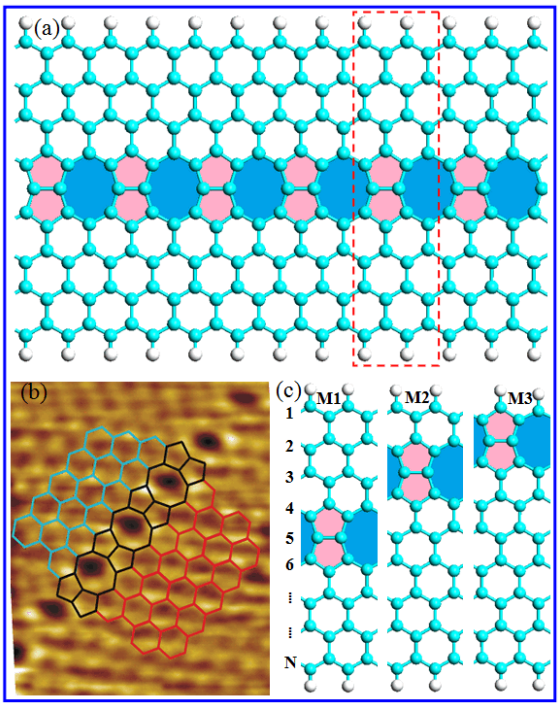

Figure 1. (a) The structural model of the relaxed ZGNR with an extended topological line defect, the line defect consists of one octagon (filled by blue) and a pair of pentagons (filled by red) periodically repeated along the edge direction. All edge carbon atoms are saturated with hydrogen atoms, the blue (white) spheres represent C (H) atoms, and the area surrounded by the red rectangle is the chosen unit supercell. (b) Scanning tunneling microscope image of the line defect in graphene and superimposed defect model (image adapted from Ref. [28]). (c) M1, M2 and M3 are the unit supercell used in the present calculations, respectively. The left number N is the number of zigzag carbon chains of ZGNRs. M1 corresponds to a line defect just located at the center, M2 and M3 correspond to models with the next-closest and closest line defects to the zigzag edge, respectively.

3. Results and discussion

We first investigate the binding energy and compare it with that of the pristine ZGNR in order to clarify the structural stability of the ZGNR with 558-defect. Here, the binding energy is defined as $E_b = \left(E_T - n_C E_C - n_H E_H\right)/\left(n_C + n_H\right)$, where E_T, E_C and E_H are the total energy of the investigated system, a C atom and a H atom, respectively. n_C and n_H are the number of C atoms and H atoms, respectively. For the case of *N*=9, the calculated binding energies of M1, M2 and M3 are -8.921eV, -8.914eV and -8.912eV, respectively. Which are comparable with the case of the pristine 9-ZGNR (-9.018eV), it indicates the structure of the ZGNR with 558-defect line is very stable as ZGNR. Then we calculate the total energies (E) of paramagnetic (PM), ferromagnetic (FM) and antiferromagnetic (AFM) configurations for 9-ZGNR, M1, M2, and M3, respectively. The calculated E display the following regularities: for 9-ZGNR, M1 and M2, $E_{AFM} < E_{FM} < E_{PM}$; for M3, $E_{AFM} = E_{FM} < E_{PM}$. It indicates the ground states of 9-ZGNR, M1 and M2 are all AFM configurations, but that of M3 is FM configuration.

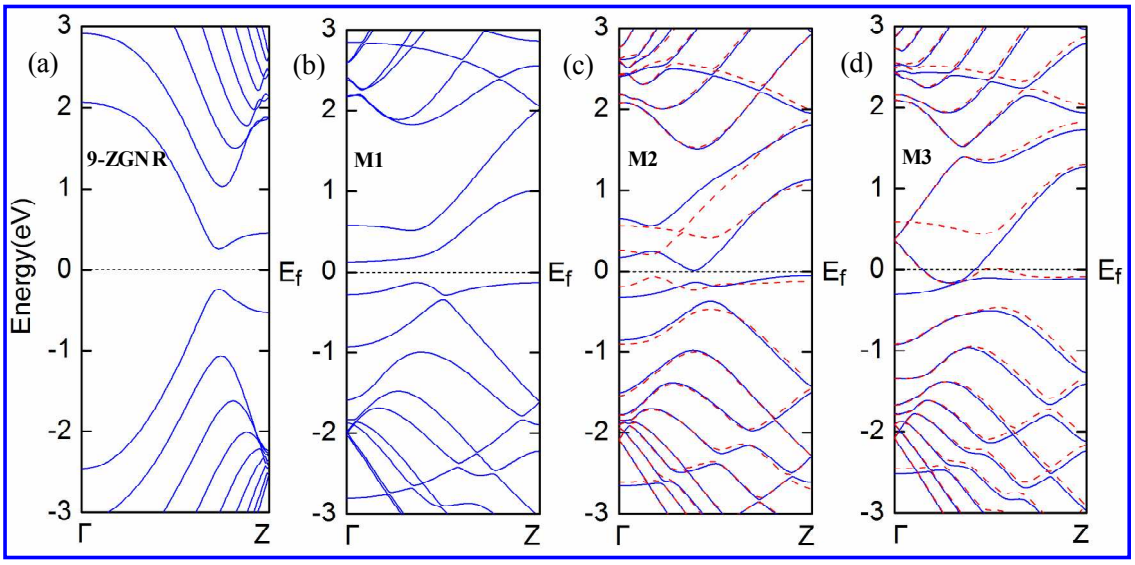

Figure 2. The spin-polarized band structures of the ZGNRs at the ground state (majority spin, solid line; minority spin, dashed line). (a) for the pristine 9-ZGNR, (b), (c), and (d) for M1, M2, and M3, respectively. The Fermi level is set to zero. Obviously, the band structures of the ZGNRs with line defect are spin split except line defect just located at the center.

We now investigate the electronic band structures of the ZGNR and M1-M3 at the ground state, as shown in **figure 2** (a)–2(d). Two important features can be viewed: (i) For 9-ZGNR and M1, the energy bands of majority spin and minority spin are degenerate completely. Conversely, for M2 and M3, the energy bands are all split obviously, and some bands get across the Fermi level in M3, this phenomenon implies the intense spin-polarization occurring and 558-defect-9-ZGNRs are all ferrimagnetic or ferromagnetic except line defect just located at the center. (ii) For 9-ZGNR and M1, there is a about 0.5eV and 0.25eV energy gap between the valence band (VB) and the conduction band (CB), respectively. So they are semiconductor. But for M2, there is almost a zero band gap for the majority spin, but a small band gap for the minority spin. This means it is half-metallic state. For M3, there is no band gap for either majority spin or minority spin. Thus it is metallic state obviously. It suggests that the ground state of 558-defect-9-ZGNR can be changed from an initial semiconductor to a half-metallic state or a metallic state just by shifting the position of line defect from the center to edge.

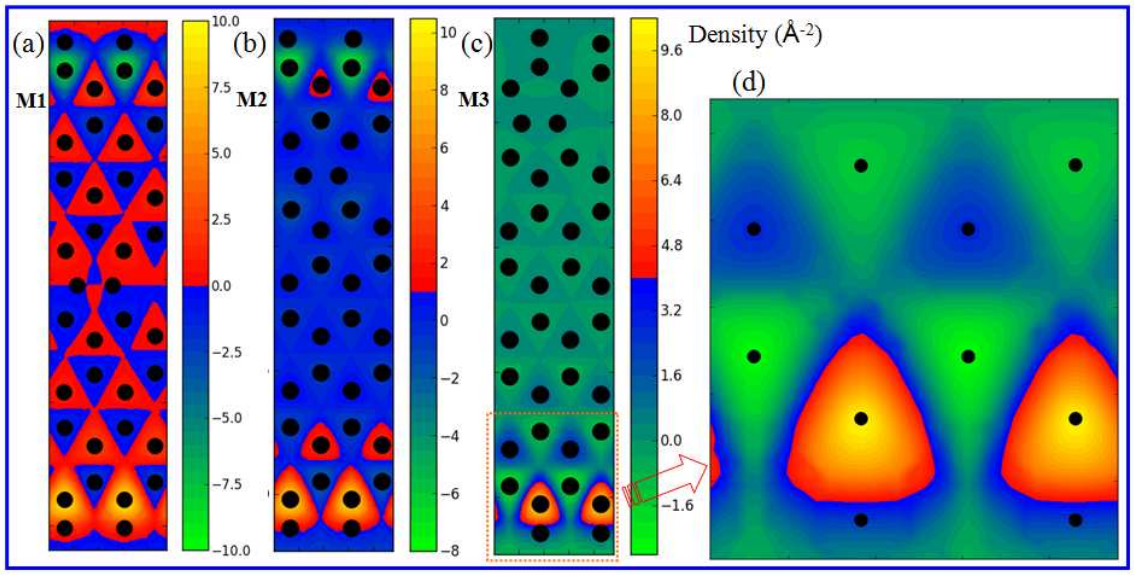

Figure 3. (a), (b) and (c) Cut plane plots of the spin polarization density (ρ↑-ρ↓) of the 558-defect-9-ZGNRs at ground state for M1, M2 and M3, respectively. (d) The enlarged view for the area surrounded by the red rectangle in (c). The filled black circles indicate the atom positions. The positive/negative numbers in the bar indicate majority/minority spin density, respectively.

To know the spin-polarization of ZGNRs with line defect, we calculate the spin polarization density (SPD) ρ↑-ρ↓ for 558-defect-9-ZGNRs at ground state, and give the density averaged in the direction perpendicular to the ribbon plane for M1, M2 and M3 in **figure 3** (a)–3(c), respectively. Here, the majority spin and minority spin are labeled as ↑ and ↓, respectively, and the electron density is denoted as ρ. From figure 3, we can observe that the SPD of the bottom edges for 558-defect-9-ZGNRs is of majority spin, with a significant larger value. The SPD of the top edge for the minority spin becomes weaker gradually to zero as the line defect position moves from the center to edge, and the SPD are very weak nearly to zero in other regions except both edges. It shows that the 558-defect-9-ZGNRs exhibit an obvious spin-polarization and can be transformed from AFM to ferrimagnetism, and to FM state because this intrinsic feature is sensitive to the position of line defect.

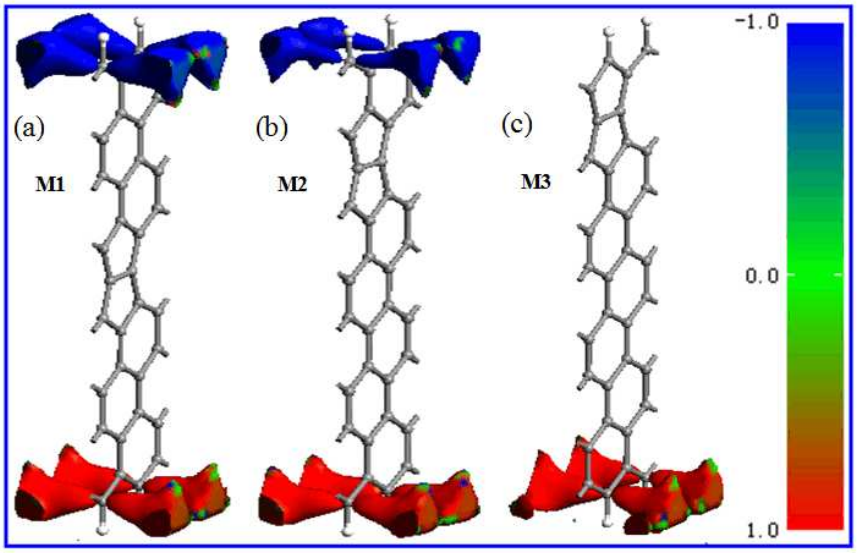

Figure 4. (a), (b) and (c) The spatial distributions of spin-polarized degree at ground state for M1, M2 and M3, respectively. The red/blue colors indicate the areas where there is a surplus of majority/ minority spin, respectively.

To further analyze the spin-polarization for ZGNRs with line defect, we define the spin-polarized degree *P* as:

$$P = \frac{\rho\uparrow - \rho\downarrow}{\rho\uparrow + \rho\downarrow} \quad (2)$$

The P is a relative spin polarization; it varies from -1 to 1. We plot the isosurface of P for M1, M2, and M3 in **figure 4**(a)–4(c), respectively. It clearly shows that intense spin-polarization occurs at edge C atoms of 558-defect-9-ZGNRs, the ground state of M1 has an antiferromagnetic spin configuration in both edges, where the total net spin is zero. While M2 and M3 have a ferrimagnetic and ferromagnetic spin configurations in edges, respectively. Moreover, these edge states are extremely sensitive to a line defect, the minority spin-polarized degree are significantly weaken and down to zero as the line defect position shifts from center to edge of nanoribbons. It suggests that the 558-defect plays an obvious inhibitory effect on the spin-polarization.

The above results show that a long-range ferromagnetic ordering can be created by employing a line defect located at one edge of ZGNR (see figure 3(c) and 4(c)). Next, we investigate the strength and stability of magnetism about ZGNRs with line defect. Two related physical parameters are magnetic moment (M) and Curie temperature (T_C). T_C can be estimated by using the mean-field theory and Heisenberg model [35-37],

$$T_C = \frac{2\Delta E}{3K_B N_C} = \frac{2\left(E^{GS+1} - E^{GS}\right)}{3K_B N_C} \quad (3)$$

where ΔE is the energy difference between an upper magnetic stable state (GS+1) and the magnetic ground state (GS) per unit cell, i.e. $\Delta E = E^{GS+1} - E^{GS}$. The E^{GS+1} and E^{GS} are corresponding to the energy of ferromagnetic and antiferromagnetic state (E_{FM} and E_{AFM}) for ZGNR, M1 and M2, but they are the energy of paramagnetic and ferromagnetic state (E_{PM} and E_{FM}) for M3, respectively. K_B is the Boltzmann constant. N_C is the number of the magnetic C atoms per unit cell. The calculated M at ground state for ZGNR, M1, M2, and M3 are shown in **figure 5** (a). We can find that, in despite of N, the M of M3 for each N is much stronger than that of the other three cases. The calculated T_C are shown in figure 5 (b) and these results are in good agreement with other DFT studies of similar systems [38–39]. We can also find that, in despite of N, the T_C of M3 for each N is much higher than that of

the other three cases. This can be explained from the M3 that exhibits a ferromagnetic ground state induced by the presence of the edge line defect, resulting in a quite large exchange energy. Most importantly, the edge line defect makes the magnetism of ZGNR changes from the pure spin AFM to FM with T_C next to room temperature such as 276 K. It suggests that employing the 558 line defect located at one edge of the ribbon while the other edge remains in an ideal zigzag shape might be an effective method to enhance the magnetism stability of ZGNR.

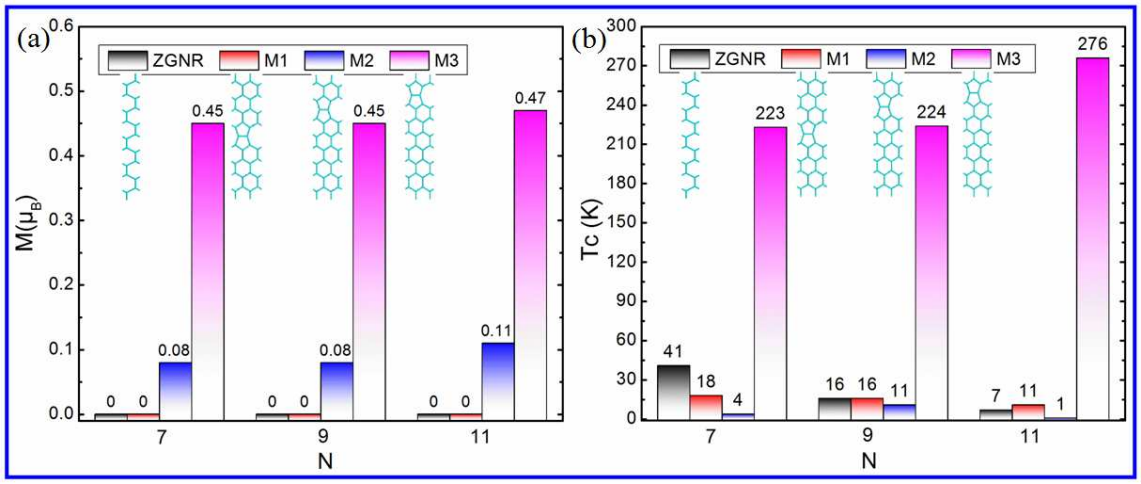

Figure 5. (a) and (b) Magnetic moment (M) and Curie temperature (T_C) of ZGNRs with line defect, respectively. N is the number of zigzag carbon chains of ZGNR. The insets in panel illustrate one exemplary unit supercell model for ZGNR, M1, M2 and M3, respectively.

We now turn to investigate the impact of line defect on the spin transport for ZGNRs. The spin-resolved current-voltage characteristics for 9-ZGNR, M1, M2 and M3 are presented in **figure 6**(a)–6(d), respectively. It can be seen that, for pristine ZGNR, the majority spin-transport is equivalent to the minority spin-transport, both the majority and minority spin electronic conductions comply with Ohm's Law of resistance, and the corresponding current-voltage characteristics in figure 6(a) are all straight lines and completely overlapping. But for 558-defect-9-ZGNRs, the impacts of line defect on majority and minority spin-transport are distinct, when the line defect position shifts from center to edge of nanoribbons, the minority-spin current becomes smaller significantly, in contrast, the

majority-spin current increases. This can be understood from the minority spin-transport pathway becoming narrower while the majority spin-transport pathway getting wider apparently as the line defect position shifts from center to edge of nanoribbons. It suggests that the spin-transport can be tuned by varying the line defect position, the line defect near the edge acts as conductors to majority spin-transport but as insulators to the opposite minority spin-transport, which generate a spin-filter effect.

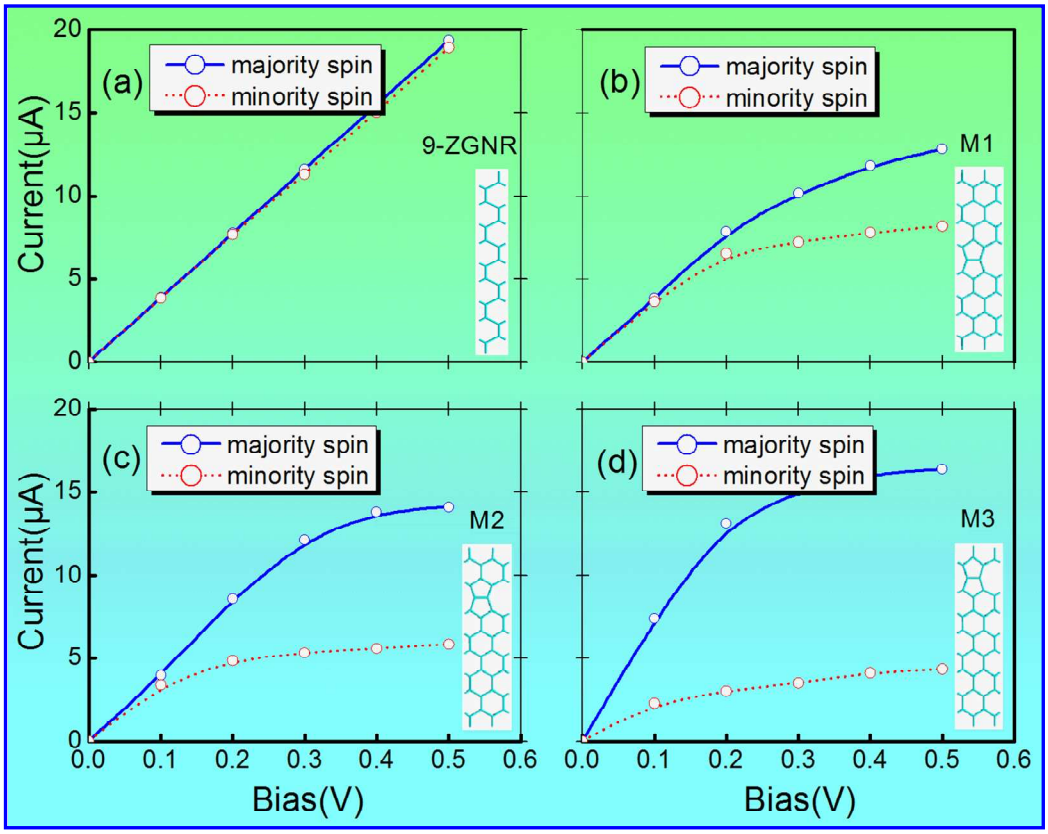

Figure 6. The spin-resolved current-voltage characteristics of defective ZGNR systems for N=9. (a), (b), (c) and (d) are describe for pristine ZGNR, M1, M2 and M3, respectively. Majority spin, solid line; minority spin, dashed line. The insets of (a) – (d) show the corresponding models of unit supercells.

To clearly reveal that the 558-defect-9-ZGNR systems can generate spin-filter effect, a way to compare the differences of spin-filter effect between the ribbons is to calculate the spin-filter efficiency (SFE) η, which is defined at zero bias as

$$\eta = \left| \frac{T\uparrow(E_f) - T\downarrow(E_f)}{T\uparrow(E_f) + T\downarrow(E_f)} \right| \times 100\%, \quad (4)$$

where $T\uparrow$ (E_f) and $T\downarrow$(E_f) represent the transmission coefficients of the majority and minority spin channels at the Fermi level E_f, respectively.

Since the spin-filter effect at finite bias is more valuable for applications than that at zero bias. We define the spin-filter efficiency (SFE) η at finite bias as

$$\eta = \left| \frac{I\uparrow - I\downarrow}{I\uparrow + I\downarrow} \right| \times 100\% \ , \quad (4)$$

where $I\uparrow$ and $I\downarrow$ represent the spin-resolved currents of the majority and minority spins at finite bias, respectively.

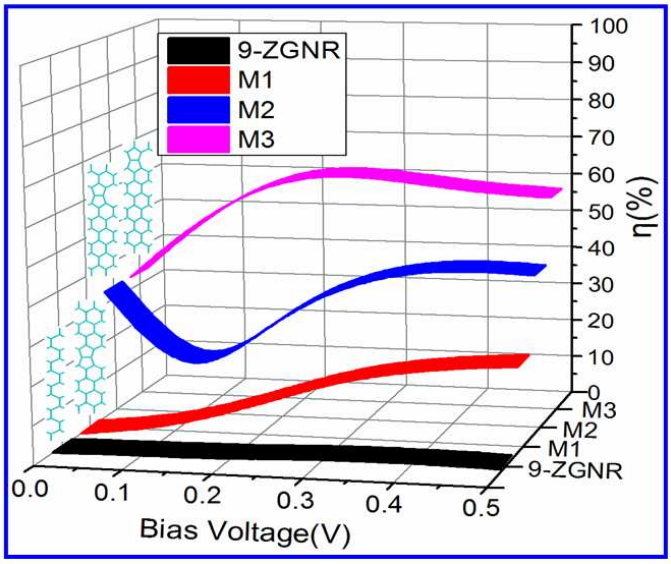

Figure 7. Spin-filter efficiency (η) of defective ZGNR systems as functions of bias voltage and line defect position. The insets in the left panel show the corresponding models of unit supercells.

The calculated SFE (η) of 558-defect-9-ZGNR systems are shown in **figure 7**. We can find the η is extremely sensitive to the line defect position and bias voltage (V_b), the η is improved remarkably with the line defect shifting to edge, the η of M3 is the most excellent one (represented by pink in figure 7), and changes within 50%～60% as $0.1 \leq V_b \leq 0.5$V. We also find that the SFE (η) of ZGNRs with N = 7, 11 display similar behaviors roughly as that of N = 9. It suggests that a stable and high-performance spin-filter device might be designed based on ZGNR with line defect closest to the zigzag edge.

4. Conclusions

Based on first-principles methods, the spin-dependent electronic properties for zigzag-edge graphene nanoribbons (ZGNRs) with a line defect are investigated and are compared to the results for ZGNR without line defect. Results show that the edge carbon atoms of the defective ZGNRs exhibit intense spin-polarization, and the spin-polarization and spin-transport are sensitive to the position of line defect. The defective ZGNRs can realize a transition from antiferromagnetism to ferrimagnetism and ferromagnetism via varying the position of line defect from the center to the zigzag edge of nanoribbons. And the ground state can be tuned from an initial semiconductor to a half-metallic state and a metallic state. In addition, the spin-transport can be tuned by varying the line defect position, the line defect near the edge acts as conductors to majority spin-transport but as insulators to the opposite minority spin-transport, which generates a spin-filter effect. More importantly, when the line defect is located the one edge, the defective ZGNRs exhibit the long-range magnetic ordering at edges with a high Curie temperature up to 276K, and the defective ZGNR system can generate high-performance spin-filter effect in the large bias range, 0.0～0.5V. Such a sensitive modulation for the spin-polarization and spin-transport holds great promise for applications of the graphene-based systems in nano-scale spintronic devices.

Acknowledgments

This work was supported by the National Natural Science Foundation of China (Grant Nos. 61371065, 61101009, and 61201080), the Scientific Research Fund of Hunan Provincial Education Department (Grant No. 14A013), the PhD Research Foundation of Changsha University of Science and Technology, the construct program of the key discipline in Hunan Province, and aid program for Science and Technology Innovative Research Team in Higher Educational Institutions of Hunan Province.

References

[1] Y. W. Son, M. L. Cohen, and S. G. Louie, *Nature*, 2006, **444**, 347–349.

[2] K. Nomura and A. H. MacDonald, *Phys. Rev. Lett.*, 2006, **96**, 256602.

[3] L. Brey, H. A. Fertig, and S. Das Sarma, *Phys. Rev. Lett.*, 2007, **99**, 116802.

[4] K. S. Novoselov, Z. Jiang, Y. Zhang, S. V. Morozov, H. L. Stormer, U. Zeitler, J. C. Maan, G. S. Boebinger, P. Kim, and A. K. Geim, *Science*, 2007, **315**, 1379.

[5] O. V. Yazyev and L. Helm, *Phys. Rev. B*, 2007, **75**, 125408.

[6] W. L. Wang, S. Meng, and E. Kaxiras, *Nano Lett.*, 2008, **8**, 241–245.

[7] T. Nikolaos, J. Csaba, P. Mihaita, T. J.Harry, and B. J. V. Wees, *Nature*, 2007, **448**, 571–574.

[8] W. Han and R. K. Kawakami, *Phys. Rev. Lett.*, 2011, **107**, 047207.

[9] D. H. Hernando, F. Guinea, and A. Brataas, *Phys. Rev. Lett.*, 2009, **103**, 146801.

[10] K. M. McCreary, A. G. Swartz, W. Han, J. Fabian, and R. K. Kawakami, *Phys. Rev. Lett.*, 2012, **109**, 186604.

[11] S. A. Wolf, D. D. Awschalom, R. A. Buhrman, J. M. Daughton, S. V. Molnar, M. L. Roukes, A. Y. Chtchelkanova, and D. M. Treger, *Science* 2001, **294**, 1488–1495.

[12] I. Zutic, J. Fabian, and S. D. Sarma, *Rev. Mod. Phys.*, 2004, **76**, 323–410.

[13] C. Chappert, A. Fert, and F. V. D. Nguyen, *Nat. Mater.* 2007, **6**, 813–823.

[14] L. Tapasztó, G. Dobrik, P. Lambin, and L. P. Biró, *Nat. Nanotechnol.* 2008, **3**, 397–401.

[15] S. S. Datta, D. R. Strachan, S. M. Khamis, and A. T. C. Johnson, *Nano Lett.* 2008, **8**, 1912–1915.

[16] C. Berger, Z. Song, X. Li, X. Wu, N. Brown, C. Naud, D. Mayou, T. Li, J. Hass, A. N. Marchenkov, E. H. Conrad, P. N. First, and W. A. de Heer, *Science*, 2006, **312**, 1191–1196.

[17] Y. W. Son, M. L. Cohen, and S. G. Louie, *Phys. Rev. Lett.*, 2006, **97**, 216803.

[18] H. Lee, Y. W. Son, N. Park, S. Han, and J. Yu, *Phys. Rev. B*, 2005, **72**, 174431.

[19] N. D. Mermin and H. Wagner, *Phys. Rev. Lett.*, 1966, **17**, 1133.

[20] J. Kunstmann, C. Özdoğan, A. Quandt, and H. Fehske, *Phys. Rev. B*, 2011, **83**, 045414

[21] K. Sawada, F. Ishii, M. Saito, S. Okada, and T. Kawai, *Nano Lett.*, 2009, **9**, 269–272.

[22] K. Sawada, F. Ishii, and M. Saito, *Phys. Rev. B*, 2010, **82**, 245426.

[23] J. A. Yan and M. Y. Chou, *Phys. Rev. B*, 2010, **82**, 125403.

[24] G. P. Tang, J. C. Zhou, Z. H. Zhang, X. Q. Deng, and Z. Q. Fan, *Carbon*, 2013, **60**, 94–101.

[25] Z. Li, W. Zhang, Y. Luo, J. Yang, and J. G. Hou, *J. Am. Chem. Soc.*, 2009, **131**,

6320–6321.

[26] B. Xu, J. Yin, Y. D. Xia, X. G. Wan, K. Jiang, and Z. G. Liu, *Appl. Phys. Lett.*, 2010, **96**, 163102.

[27] G. P. Tang, Z. H. Zhang, X. Q. Deng, Z. Q. Fan, Y. C. Zeng, and J. C. Zhou. *Carbon*, 2014, **76**, 348–356.

[28] J. Lahiri, Y. Lin, P. Bozkurt, I. I. Oleynik, and M. Batzill, *Nature Nanotech.*, 2010, **5**, 326–329.

[29] Q. Q. Dai, Y. F. Zhu, and Q. Jiang. *J. Phys. Chem. C* 2013, **117**, 4791–4799

[30] Q. Q. Dai, Y. F. Zhu, and Q. Jiang. *Phys. Chem. Chem. Phys.* 2014, **16**, 10607–10613

[31] S. S. Alexandre, A. D. Lúcio, A. H. C. Neto, and R. W. Nunes. *Nano Lett.*, 2012, **12**, 5097–5102.

[32] C. Su, H. Jiang, and J. Feng. *Phys. Rev. B*, 2013, **87**, 075453.

[33] X. L. Sheng, H. J. Cui, F. Ye, Q. B. Yan, Q. R. Zheng, and G. Su. *J. Appl. Phys.*, 2012, **112**, 074315.

[34] O. V. Yazyev and S. G. Louie, *Nature Mater.*, 2010, **9**, 806–809.

[35] P. Kurz, G. Bihlmayer, and S. Blüge, *J. Phys.: Condens. Matter*, 2002, **14**, 6353–6371.

[36] T. Hynninen, H. Raebiger, and J. Boehm, *Phys. Rev. B*, 2007, **75**, 125208.

[37] J. Kunstmann, C. Özdoğan, A. Quandt, and H. Fehske, *Phys. Rev. B*, 2011, **83**, 045414.

[38] M. Sepioni, R. R. Nair, S. Rablen, J. Narayanan, F. Tuna, R. Winpenny, A. K. Geim, and I. V. Grigorieva, *Phys. Rev. Lett.*, 2010, **105**, 207205.

[39] O. V. Yazyev and M. I. Katsnelson, *Phys. Rev. Lett.*, 2008, **100**, 047209.